

1 **SUPPLEMENTARY MATERIAL**

2 **Variability of Black Carbon mass concentration in surface snow at Svalbard**

3 Michele Bertò<sup>1#</sup>, David Cappelletti<sup>2,7</sup>, Elena Barbaro<sup>1,3</sup>, Cristiano Varin<sup>1</sup>, Jean-Charles Gallet<sup>4</sup>,  
4 Krzysztof Markowicz<sup>5</sup>, Anna Rozwadowska<sup>6</sup>, Mauro Mazzola<sup>7</sup>, Stefano Crocchianti<sup>2</sup>, Luisa Poto<sup>1,3</sup>,  
5 Paolo Laj<sup>8</sup>, Carlo Barbante<sup>1,3</sup> and Andrea Spolaor<sup>1,2\*</sup>.

6

7 <sup>1</sup>Ca' Foscari University of Venice, Dept. Environmental Sciences, Informatics and Statistics, via  
8 Torino, 155 - 30172 Venice-Mestre, Italy;

9 <sup>2</sup>Università degli Studi di Perugia, Dipartimento di Chimica, Biologia e Biotecnologie, Perugia, Italy;

10 <sup>3</sup>CNR-ISP, Institute of Polar Science – National Research Council –via Torino, 155 - 30172 Venice-  
11 Mestre, Italy;

12 <sup>4</sup>Norwegian Polar Institute, Tromsø, Norway.

13 <sup>5</sup>University of Warsaw, Institute of Geophysics, Warsaw, Poland;

14 <sup>6</sup>Institute of Oceanology, Polish Academy of Sciences, Sopot, Poland;

15 <sup>7</sup>CNR-ISP, Institute of Polar Science – National Research Council – Via Gobetti 101, Bologna;

16 <sup>8</sup>Univ. Grenoble-Alpes, CNRS, IRD, Grenoble-INP, IGE, 38000 Grenoble, France

17

18 <sup>#</sup> Now at Laboratory of Atmospheric Chemistry, Paul Scherrer Institute, 5232 Villigen PSI,  
19 Switzerland

20

21

22

23

24

25

26

27

28

29

30

31

32

33

34

35

36

### 37 **1. Details of the statistical analyses**

38 The two multiple linear regression models were fitted on the logarithm scale because the  
39 distribution of rBC concentrations in both the experiments is characterized by a significant skewness.  
40 Coarse mode particles number concentrations and conductivity were also log-transformed to linearize  
41 their relationships with log(rBC). Graphical inspection of residuals plots and normal probability plots  
42 confirmed that after the logarithm transformations, the regression models meet the assumptions of  
43 linearity, constant error variance (called *homoscedasticity* in the statistical literature) and normal  
44 errors. The regression model fitted on the 85-days (daily sampling resolution) experiments is:

45

$$46 \log(\text{rBC}) = \beta_0 + \beta_1 \log(\text{dust}) + \beta_2 \text{eBC} + \beta_3 \text{temp} + \beta_4 \text{snow} + \beta_5 \text{SWR} + \beta_6 \log(\text{cond}) + \epsilon$$

47

48 In the regression model ‘dust’ indicates coarse mode particles number concentrations, ‘temp’ is  
49 the snow temperature, ‘snow’ is an indicator for the solid precipitation, ‘SWR’ is solar incoming  
50 shortwave radiation, ‘cond’ is the conductivity and  $\epsilon$  is a normal error. In the 3-days experiment  
51 (hourly resolution), the model includes also trigonometric components  $\sin(2\pi \text{ hour}/24)$  and  $\cos(2\pi$   
52  $\text{ hour}/24)$  to account for the hourly periodicity of the incoming solar energy. The statistical analyses  
53 were performed with the statistical language R (R Core Team, 2020).

54

### 55 **2. Calibration of the SP2**

56 The empirical calibration of the SP2, performed using size selected fullerene soot particles is linear up  
57 to 500 nm, and the assumption is that it is also linear beyond that size (and the corresponding mass).  
58 However, when a massive particle enters the laser beam the incandescence signal might saturate the  
59 detector; therefore, in this analysis only the particles below 700 nm were considered. The evaluation  
60 of the BC mass for the samples showing a BC geometric mean mass equivalent diameter above  
61 300/400 nm, might therefore be more influenced resulting in an underestimation of the mass.  
62 However, the evaluation of the missing mass is beyond the scope of this manuscript and require  
63 further analyses. The losses of mass due to the presence of undetected small particles, below 80/70  
64 nm of MED, is not significant given that the geometric mean of the MED of the mass size  
65 distributions is always above 150 nm.

66

### 67 **3. Possible interferences during the SP2 rBC mass concentration in Arctic snow**

68 The surface snow of the Svalbard archipelago is normally characterized by high content of sea salt  
69 particles, for example those containing Na, due to its geographical position surrounded by the ocean.  
70 The Na concentration in the samples analyzed in this work is, on average, about 500 ng g<sup>-1</sup>. We  
71 cannot exclude that the rBC mass concentration variability for the 85-days experiment presented in  
72 this work might have been slightly influenced by the Na content (tracer of sea salt deposition),

73 however any clear relation appeared from the comparison between the rBC and the Na mass  
74 concentrations during the “85 days” experiment (Fig. SI 3). As a precaution, all samples from the 3-  
75 days experiments were diluted five times with Milli-Q water prior to the SP2 analyses. The SP2  
76 instrumental performances during the analyses, in terms of laser power and incandescence signal  
77 quality, were monitored and constant. At the best of our knowledge, no study focusing on the possible  
78 effects of the Na particles on the rBC mass concentration retrieved from the SP2 has been published  
79 in the literature. Further analyses of snow samples collected in areas characterized by a high influence  
80 of marine-like aerosols could shed light on the effects of salt particles on the rBC mass and number  
81 concentration via SP2 measurements, as well as establishing a shared procedure to avoid measuring  
82 artifacts.

83 Moreover, mineral dust particles might have an influence on the SP2 measurements, depending on  
84 their chemical and physical properties. Currently, the literature lacks investigation on these specific  
85 SP2-mineral dust particles interactions. However, a few studies on snow and ice samples measured  
86 with an SP2 take the assumptions that mineral dust particles are not detected by the SP2 as  
87 incandescence signals, but only as scattering signals (Kaspari et al., 2011). Recent studies, based on  
88 atmospheric measurements suggest that the SP2 rBC mass concentration measurement can potentially  
89 be interfered by the presence of metals and metals-oxide (Moteki et al., 2017), of volcanic ashes or of  
90 dust (Kupiszewski et al., 2016).

#### 91 **4. Ancillary measurements for the 3-days samples: Na, Mn, EC, OC**

92 Ancillary data were measured/gathered for the 3-days experiment in order to strengthening  
93 the interpretations even though they were not considered in the statistical exercise. The Mn  
94 concentrations are considered to be a good proxy for mineral dust aerosols (Baker et al., 2006). In  
95 **Errore. L'origine riferimento non è stata trovata.**4 the Mn concentration profile was compared  
96 with that of the coarse mode particles concentration showing a very similar behavior and suggesting a  
97 common source. Despite some differences, a similar pattern is also clearly visible for all the various  
98 chemical species.

99 Every six hours a surface snow sample was collected in parallel to that of the hourly  
100 sampling. These samples water volume was of about  $1618 \pm 290 \text{ mL cm}^3$  and they were used for TC,  
101 EC and OC measurement, and the results are shown in Fig. SI 4. A different profile is shown for the  
102 three compounds compared to that of the rBC mass concentration. As reported above the two  
103 measuring techniques are different and, in particular, the size range of particles detected by the two  
104 instruments is different, from 80 to 600 nm for the SP2 whereas a much broader dimensional  
105 spectrum for the Sunset, potentially explaining part of the observed difference. Interestingly, the EC  
106 daily values increased of one order of magnitude, from 1 to  $10 \mu\text{g l}^{-1}$ , during the sampling period,  
107 showing a maximum during the precipitation episode. For more info and results about the comparison  
108 between rBC and EC snow/ice measurement check Sigl et al. (2018). On the contrary, the OC

109 atmospheric concentration showed a decreasing trend showing the highest values at the beginning of  
110 the sampling period and the lowest at the end, similarly to the atmospheric eBC behavior.  
111 Remarkably, the highest OC concentration was found in the same sample were the highest  
112 concentration of all the other measured compounds was found (at the very beginning of the snow  
113 episode) suggesting a common atmospheric scavenging process (although not above the average for  
114 the rBC mass concentration).

## 115 **5 Conductivity and sodium/manganese concentrations measurements**

116 The total conductivity of the melted snow was measured in parallel with a simple  
117 conductivity Micro-Cell. The water conductivity depends from the number of soluble anions and  
118 cations in the snow, as for instance sea salt sodium. Concentrations of sodium (Na) and manganese  
119 (Mn) were also determined as tracer of sea spray emission and dust deposition by Inductively Coupled  
120 Plasma Sector Field Mass Spectrometry (ICP-SFMS; Element2, ThermoFischer, Bremen, Germany)  
121 equipped with a cyclonic Peltier-cooled spray chamber (ESI, Omaha, USA). The sample flow was  
122 maintained at  $0.4 \text{ mL min}^{-1}$ . Detection limits, calculated as three times the standard deviation of the  
123 blank, were  $0.5 \text{ ng g}^{-1}$  for  $^{23}\text{Na}$  and  $0.3 \text{ ng g}^{-1}$  for Mn. The residual standard deviation (RSD) for Na  
124 and Mn ranged between 2–5%.

125

## 126 **6 Back trajectories calculation and Potential Source Contribution Function analysis**

127 Air mass back-trajectories (BT) were calculated using the NOAA ARL HYSPLIT 4 rev. 513  
128 transport model (Stein et al., 2015). Global Data Assimilation System (GDAS) meteorological input  
129 fields with  $0.5 \times 0.5$  degree resolution and a propagation time of 240 hours was employed. The  
130 trajectories were calculated every hour for an endpoint of 500 m above ground level in Ny-Ålesund. A  
131 potential source contribution function (PSCF) analysis has been applied to the BTs exploiting a  
132 specifically developed FORTRAN computer code (Petroselli et al., 2018). That analysis considered  
133 BC concentration measured in the air by both AE31 and PSAP. Briefly, the method calculates the  
134 probability of finding a source of a particular pollutant on a certain region by superimposing grid cells  
135 to it and estimating the fraction of the total time spent on each cell by trajectories associated with a  
136 high concentration measured at the receptor site. The 90th percentile was used to define the high  
137 concentration limit and cells of  $3 \times 3$  degrees (lat-long) were exploited in the calculation of  
138 probabilities. Details of the PSCF methodology employed here are described in Petroselli et al.,  
139 (2018). The data of the active fires, covering the last 12 days before the sampling day, are from the  
140 MODIS active fire products (<https://firms.modaps.eosdis.nasa.gov/firemap/>), offered by NASA  
141 LANCE.

142 In order to evaluate the impact of the Eurasian fires on the measured atmospheric eBC  
143 concentrations, a thorough back-trajectories analysis was performed for both the snow-sampling  
144 periods. Results of PSCF analysis on eBC (Figures SI 1a, SI 1b and SI 1c; open-fire episodes are

145 reported in red on the map) show a clear maximum of probability over the Central Siberia, which  
 146 appears to be the major source area of eBC in this period over Ny-Ålesund. Some false positive  
 147 source areas are located in Greenland, the Queen Elisabeth Islands region and the Arctic Ocean, even  
 148 if associated to a lower probability. These artifacts are due to the persistent circulation of BTs in the  
 149 Arctic vortex. An example of BTs generating the above salient features in the PSCF plot is reported in  
 150 Figure SI 1b. Here BTs are shown to loop for few days around the Arctic at high altitudes and  
 151 afterwards to descend at lower altitudes over Siberia, just four days before reaching Ny-Ålesund on  
 152 April 22, when a clear maximum in the eBC trend has been recorded. Back trajectory analysis  
 153 supports the idea that the peaks of eBC in the atmosphere in early spring are directly correlated with  
 154 long-range transport from Eurasia, whereas the peaks in late May and June are much lower in  
 155 intensity, seemed to be more related to a Western circulation pattern.

156 The results of BT analysis for the 3-days experiment are reported in Figure SI 2, suggesting  
 157 that the air masses were persistently circulating in the polar vortex and very similar within the three  
 158 days in terms of BC atmospheric sources, physical properties and mixing state.

159

160 **Table S1.** Abakus Klotz selected dimensional bins.

Channel	Size ( $\mu\text{m}$ )	11	2.2	22	6.4
1	0.8	12	2.4	23	7.1
2	0.9	13	2.6	24	7.8
3	1	14	2.9	25	8.6
4	1.1	15	3.2	26	9.5
5	1.2	16	3.5	27	10.5
6	1.3	17	3.9	28	11.6
7	1.4	18	4.3	29	12.8
8	1.6	19	4.8	30	14.1
9	1.8	20	5.3	31	15.5
10	2	21	5.8	32	80

161

162

163

164

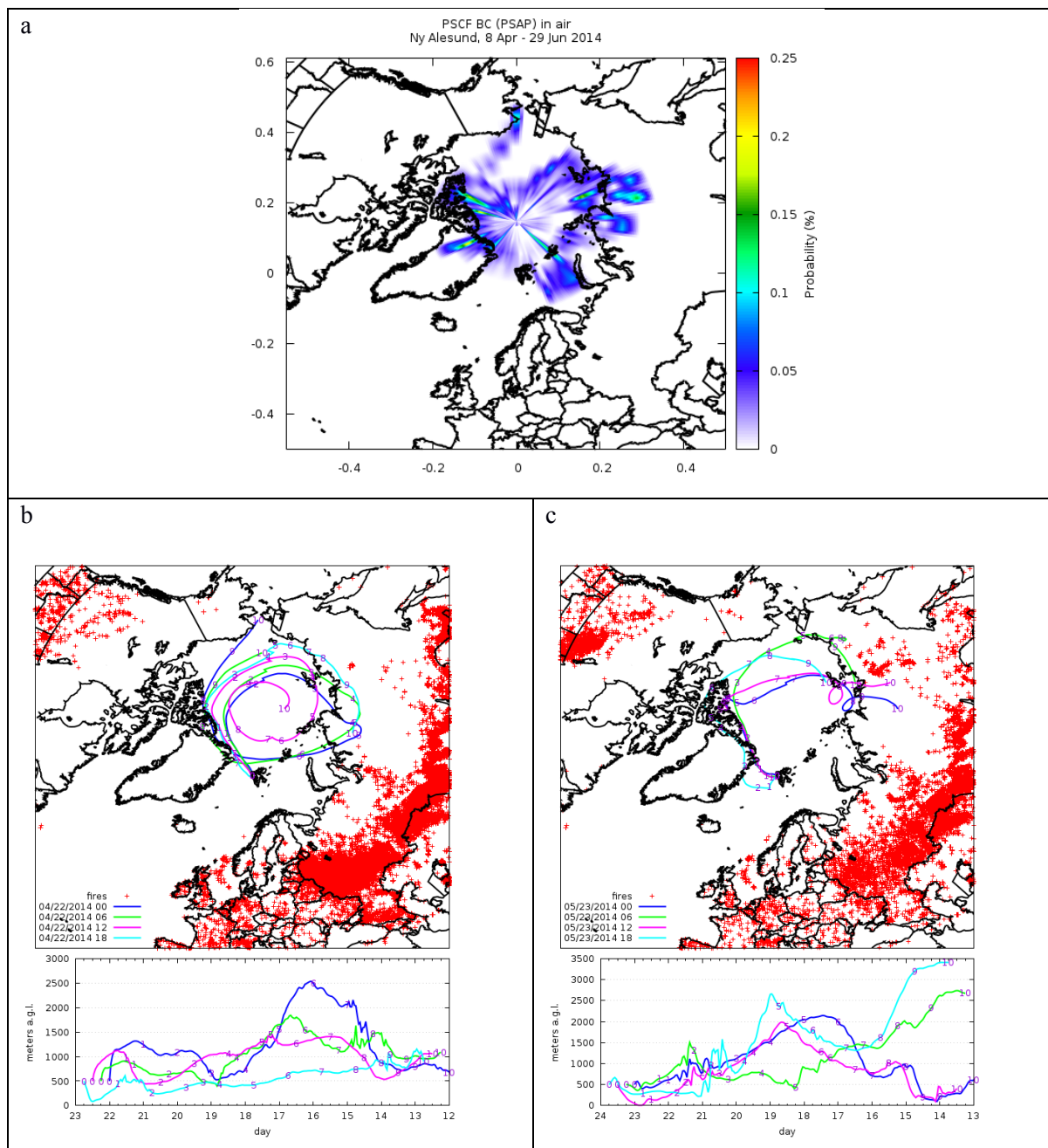
165

166

167

168

169 **Figure S1.** a) Potential source contribution function analysis (PSCF) of eBC recorded in the 85-days  
 170 experiment (8 April-29 June). 10 days back-trajectories for two selected days: b) 22 April and c) 23  
 171 May. Four BTs were calculated for the two selected days, with a 6 hours interval. The red crosses  
 172 represent the fires taking place during the last 10 days (data from the MODIS active fire products  
 173 (<https://firms.modaps.eosdis.nasa.gov/firemap>)).

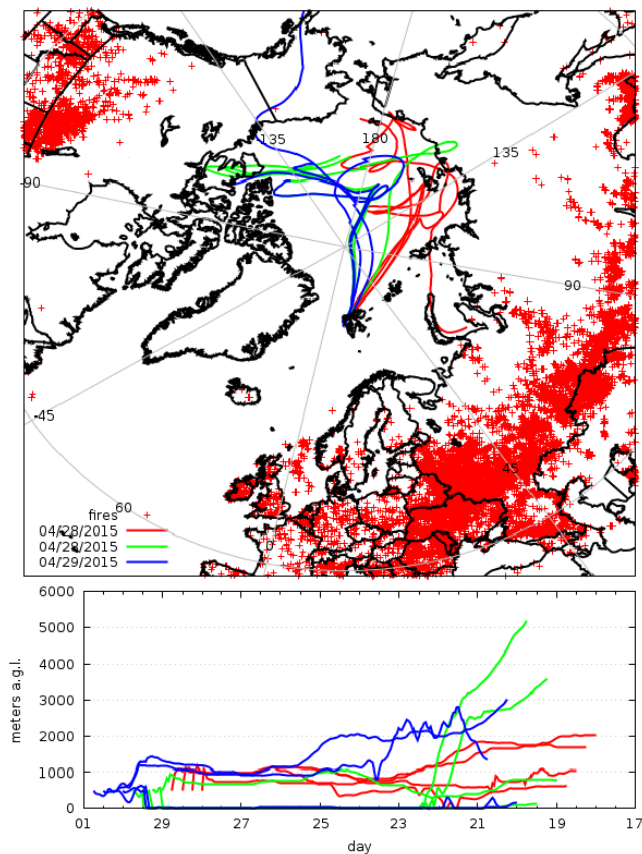


174

175

176

177 **Figure S2.** 10 days back-trajectory results for the 3-days experiment (three per day with a 8 hours  
178 interval). The red crosses represent the fires taking place during the last 10 days (data from the  
179 MODIS active fire products (<https://firms.modaps.eosdis.nasa.gov/firemap/>)).



180  
181  
182  
183  
184  
185  
186  
187  
188  
189

190 **Figure S3.** Results for the 85-days experiment from ancillary measurements. Upper panel: rBC mass  
191 concentration (gray line), Na concentration (red line) and conductivity (green line). Lower panel:  
192 atmospheric eBC mass concentration (black line) and ammonia as measured at the Zeppelin station,  
193 Svalbard (gray bars).

194

195

196

197

198

199

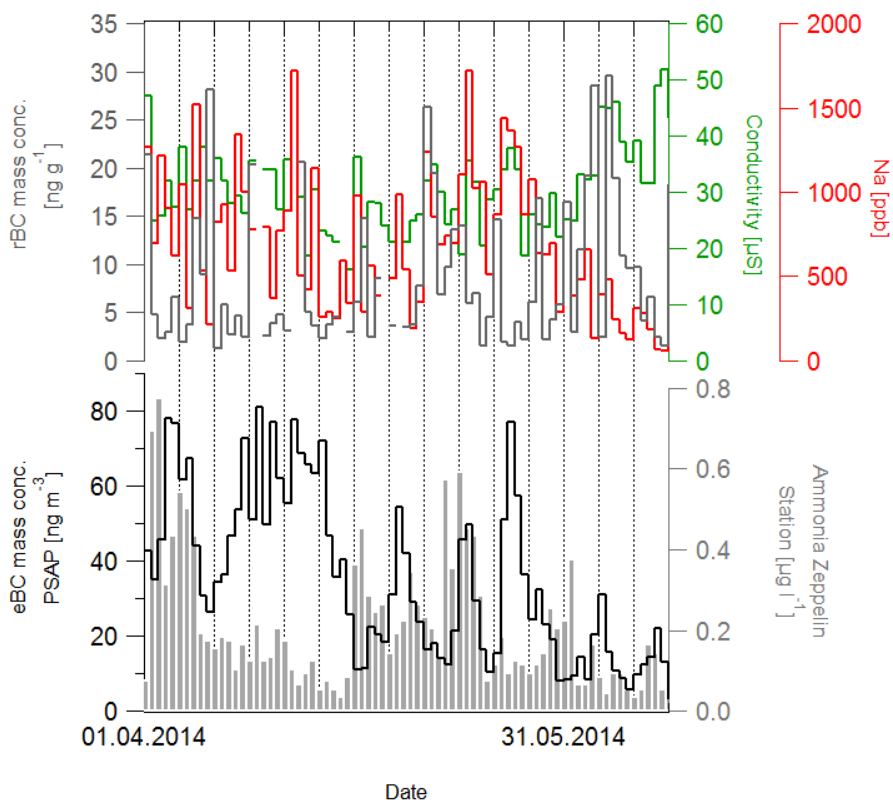
200

201

202

203

204



205

206

207

208

209

210

211

212

213

214



215 **Figure S4.** The 3-days experiments results from ancillary measurements. Uppermost panel:  
 216 manganese (Mn, dark-yellow line) mass concentration and the coarse mode particles number (blu  
 217 line). Second uppermost panel: rBC mass concentration (gray line) with sodium (Na) concentration  
 218 (red line) and conductivity (green line). Second lowermost panel: atmospheric eBC mass  
 219 concentration (black line), snow OC concentration (blue bars) and daily average of atmospheric  
 220 ammonia as measured at the Zeppelin station (gray bars). Lowermost panel: TC (red bars), OC (blue  
 221 bars) and EC (green bars) and EC daily average (black line).

222

223

224

225

226

227

228

229

230

231

232

233

234

235

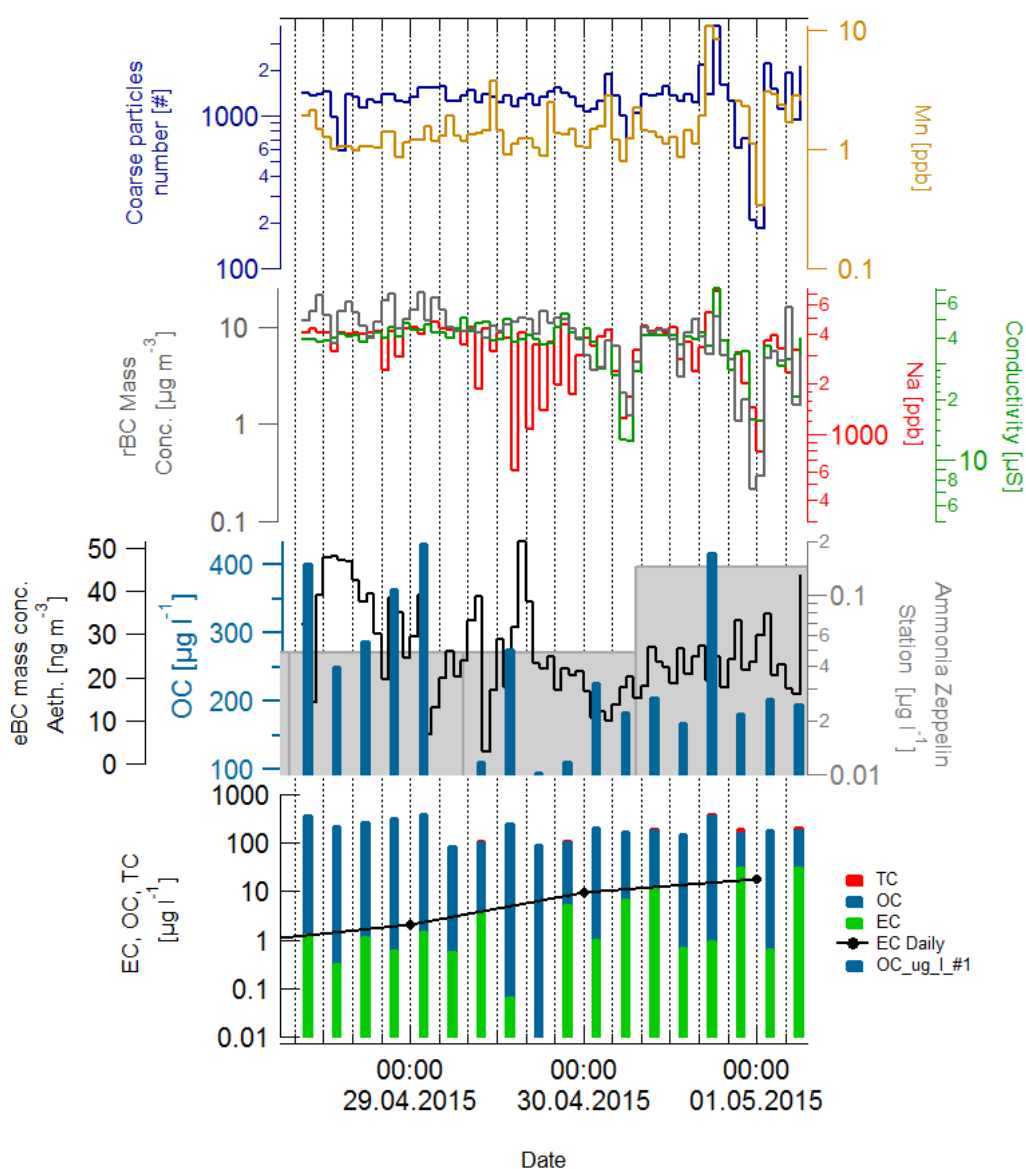
236

237

238

239

240



241 **References:**

- 242 Kaspari, S. D., Schwikowski, M., Gysel, M., Flanner, M. G., Kang, S., Hou, S. and Mayewski, P. A.:  
243 Recent increase in black carbon concentrations from a Mt. Everest ice core spanning 1860–2000  
244 AD, *Geophysical Research Letters*, 38(4), doi:10.1029/2010GL046096, 2011.
- 245 Kupiszewski, P., Zanatta, M., Mertes, S., Vochezer, P., Lloyd, G., Schneider, J., Schenk, L.,  
246 Schnaiter, M., Baltensperger, U., Weingartner, E. and Gysel, M.: Ice residual properties in mixed-  
247 phase clouds at the high-alpine Jungfrauoch site, *Journal of Geophysical Research: Atmospheres*,  
248 121(20), 12,343–12,362, doi:10.1002/2016JD024894, 2016.
- 249 Moteki, N., Adachi, K., Ohata, S., Yoshida, A., Harigaya, T., Koike, M. and Kondo, Y.:  
250 Anthropogenic iron oxide aerosols enhance atmospheric heating, *Nature Communications*, 8, 15329,  
251 doi:10.1038/ncomms15329, 2017.
- 252 Sigl, M., Abram, N. J., Gabrieli, J., Jenk, T. M., Osmont, D. and Schwikowski, M.: 19th century  
253 glacier retreat in the Alps preceded the emergence of industrial black carbon deposition on high-  
254 alpine glaciers, *The Cryosphere*, 12(10), 3311–3331, doi:https://doi.org/10.5194/tc-12-3311-2018,  
255 2018.
- 256 Petroselli, C., Crocchianti, S., Moroni, B., Castellini, S., Selvaggi, R., Nava, S., Calzolari, G.,  
257 Lucarelli, F. and Cappelletti, D.: Disentangling the major source areas for an intense aerosol  
258 advection in the Central Mediterranean on the basis of Potential Source Contribution Function  
259 modeling of chemical and size distribution measurements, *Atmospheric Res.*, 204, 67–77,  
260 doi:10.1016/j.atmosres.2018.01.011, 2018.
- 261 R Core Team: R: A language and environment for statistical computing. Vienna, Austria: R  
262 Foundation for Statistical Computing; 2020. URL <https://www.R-project.org>.
- 263 Stein, A. F., Draxler, R. R., Rolph, G. D., Stunder, B. J. B., Cohen, M. D. and Ngan, F.: NOAA's  
264 HYSPLIT Atmospheric Transport and Dispersion Modeling System, *Bull. Am. Meteorol. Soc.*,  
265 96(12), 2059–2077, doi:10.1175/BAMS-D-14-00110.1, 2015.